Photochemistry and Photobiology, 2004, 80: 89–97

Chemical and Structural Changes in Blood Undergoing Laser Photocoagulation¶

John F. Black†[1] and Jennifer Kehlet Barton*[2]

[1]Coherent Medical Group, 2400 Condensa Street, Santa Clara, CA
[2]Division of Biomedical Engineering, University of Arizona, Tucson, AZ

Received 5 March 2004; accepted 21 April 2004

ABSTRACT

The treatment of cutaneous vascular lesions (port wine stains etc.) using lasers has been guided by theories based on the "cold" or room-temperature optical properties of the hemoglobin target chromophore. We have recently presented evidence showing that under the influence of laser irradiation, the optical properties of blood *in vitro* are time and temperature dependent. Such complications are not currently subsumed into the *in vivo* theory. Here, we study the time-domain optical properties of blood undergoing photocoagulation *in vitro* using two newly developed time-resolved techniques. We also study the asymptotic effect of laser photocoagulation on the chemical and structural properties of the components of the blood matrix. We present evidence showing that the photocoagulation process involves significant changes in the optical absorption and scattering properties of blood, coupled with photothermally induced chemical and structural changes. We demonstrate the first use of a laser to deliberately generate magnetic resonance imaging contrast *in vitro*. We show that this technique offers significant potential advantages to *in vivo* intravenous chemical contrast agent injection.

INTRODUCTION

Laser therapy of cutaneous vascular disorders such as port wine stains (PWS) and telangiectases has advanced substantially during the past 20 years using the principle of selective photothermolysis, whereby a particular wavelength, pulse duration and energy are selected by examining the optical properties of the target in contrast to its surroundings (1–8). The theory has proved highly successful; however, a number of anomalous results have complicated our understanding of the process. These include observations that 590 nm light actually has a lower penetration depth than 585 nm light (7) in pig skin, despite having lower hemoglobin absorption. Clinical experiments have also shown a slightly better response with 595 nm over 600 nm in pulsed dye laser irradiation of leg telangiectasias (8), in contrast to what one would expect on the basis of the penetration depth arguments. More recently, studies of long-pulse 1064 nm irradiation of PWS have shown an all-or-nothing response (9), as opposed to a sigmoid dose–rate curve (10), along with full-thickness dermal burns in one case.

We have shown that the laser photothermal coagulation of blood *in vitro* is a complicated process involving time- and temperature-dependent changes in both optical and structural properties (11–13). We have postulated a three-stage mechanism for coagulation involving a heating phase, a primary coagulation phase involving mainly the cytoplasm of the erythrocytes and a secondary coagulation phase involving a more long-range intercellular coagulation. We have shown that a chemical change occurs in the hemoglobin at a critical temperature creating methemoglobin (met-Hb), a conformer of hemoglobin incapable of exchanging oxygen. We have measured the temperature at which these processes occur and have shown that the system can be well modeled using finite element analysis and that the denaturation is consistent with an time-dependent Arrhenius-type mechanism (12). Our time-domain results using internal laser shock heating of the erythrocytes are in excellent agreement with previous data using thermal ''bath'' heating (14–17). We have also shown how these dynamically evolving optical properties can be harnessed *in vivo* in a two-stage laser photocoagulation technique, which has shown superior efficacy to single wavelength photocoagulation in an animal model (11). Majaron and coworkers have recently demonstrated the first clinical evidence for a two-wavelength cooperative effect in clearing PWS in humans (18). Mordon and coworkers have implicated met-Hb in accounting for observations in the treatment of lower-extremity telangiectases using Nd:YAG lasers at 1064 nm (19).

In this article we build on our results using new optical probes of the *in vitro* coagulation dynamics. We have developed time- and depth-resolved optical coherence tomography (OCT) to probe the spatial evolution of the coagulum. We have also extended our spectroscopic time-domain pump-probe experiment to include wavelengths through the near infrared, which has in turn allowed us to confirm some of our earlier postulates. Finally, we have demonstrated that the ability to produce met-Hb in high concentrations in a controllable manner using a laser offers the possibility of generating magnetic resonance imaging (MRI)

¶Posted on the website on 6 May 2004
*To whom correspondence should be addressed: Division of Biomedical Engineering, University of Arizona, ECE Building 104, 1230 E. Speedway Boulevard, Tucson, AZ 85721-0104, USA. Fax: 520-621-8076; e-mail: barton@u.arizona.edu
†Current address: Reliant Technologies, 260 Sheridan Avenue, 3rd Floor, Palo Alto, CA 94306, USA.
Abbreviations: deoxy-Hb, deoxyhemoglobin; Hct, hematocrit; met-Hb, methemoglobin; OCT, optical coherence tomography; oxy-Hb, oxyhemoglobin; MRI, magnetic resonance imaging; PWS, port wine stains; RBC, red blood cell; RCIN, radiocontrast-induced nephropathy; SEM, scanning electron microscope; TE, echo time; TR, relaxation time.

contrast *in vivo*. Using these results we reinforce our earlier suggestion that the theory of selective photothermolysis as applied to vascular lesions should be extended to incorporate the time-domain effects of laser heating of the chromophore.

MATERIALS AND METHODS

Integrating sphere laser pump-probe experiments. Blood from three apparently healthy volunteers, one woman (hematocrit [hct] 44%) and two men (hct 46% and 49%) was extracted into vacuum containers containing ethylenediaminetetraacetic acid anticoagulant, chilled and used within 72 h. At the time of the experiment the blood was warmed to room temperature, gently agitated and diluted as required with isotonic saline. Washed suspensions of red blood cells (RBs) were prepared by taking whole-blood samples and repeatedly centrifuging and washing the samples in isotonic saline. Macerated RBC suspensions were prepared by taking the plasma-free RBC suspensions formed in the previous step and lysing by diluting with deionized water. Where a ''clear'' solution of oxygenated blood (oxy-Hb) was needed, the macerated mixture formed in the previous step was subjected to centrifugation and the supernatant extracted. Samples were loaded into a 200 μm pathlength demountable cuvette (20/O-G series, Starna Cells, Atascadero, CA). Each blood sample was irradiated only once. The cuvette was placed in the central sample chamber of a standard double-integrating sphere experiment detailed previously (11,20). Briefly, two integrating spheres (RT-60-SF, Labsphere, North Sutton, NH) were coupled with a sample holder. A pump beam (532 nm, 10 ms pulse duration, 3 mm spot size, variable radiant exposure, VersaPulse Cosmetic Laser [VPC™], Coherent Medical Group, Santa Clara, CA) and one of several probe beams were launched through adjacent ports of the reflectance sphere and overlapped at the sample location. The pump laser pulse energy, total reflectance of the pump laser and reflectance and transmission of the probe lasers were measured with fiber-coupled PDA-55 photodiodes (Thorlabs, Newton, NJ). Reflectance and transmission of the probe beam were also measured by wide-area photodetectors (Model #2031, New Focus, Santa Clara, CA) direct-coupled to the sphere in cases of low signal level. Interference filters were placed in front of each detector to isolate the wavelength of interest.

The residual undeflected pump beam passed through an open port in the transmission sphere and was absorbed in a beam dump. The conjugate exit port for the probe beam was either left covered, to obtain a total transmission measurement, or removed, allowing an ''undeflected'' transmission measurement to be made by placing a detector outside the rear (transmission) sphere. This measured the collimated transmission plus forward-scattered light contained within a solid cone of approximately 2.8° half-angle. In this latter configuration, it was also possible to make a ''deflected'' transmission measurement by monitoring the change in signal in the transmission sphere as a function of time. This measurement is sensitive to sample changes, causing light to be scattered out of the path of the collimated probe beam. Probe wavelengths of 594, 633, 675, 780, 820, 905, 980 and 1064 nm were used. The 594 and 633 nm probes were HeNe laser lines, and the 1064 nm probe was a diode-pumped solid-state Nd:YAG laser. The other probe wavelengths were provided by collimated (lensed) semiconductor diode lasers from a number of sources with power levels ranging from 5–20 mW. The output of the pump laser fiber face is imaged at the cuvette in the spheres, ensuring a top-hat beam profile (3 mm diameter) and, therefore, uniform illumination. The probe beams were used ''as is'' from the sources (TEM_{00} profiles with aperture diffraction rings on the diode laser sources), with the condition that the probe beams were made smaller (1–2 mm diameter) than the pump at the cuvette. The two beams are aligned to be concentric at the cuvette.

Optical coherence tomography. The OCT system is similar to one described previously (21). Briefly, the system uses a broadband fiber-coupled source at 1310 nm center wavelength and 49 nm full-width half-maximum bandwidth for a coherence length of 16 μm. The source was coupled into a fiber Michelson interferometer. The reference arm was a rapid-scanning Fourier domain optical delay line operating at 800 *a*-scans (depth scans) per second. The sample arm optics focused the light to a 16 μm spot diameter. Because the coagulation geometry can be adequately described as one dimensional within the central portion of the pump laser beam, no lateral scanning was necessary. The images presented are therefore *m*-scans (a function of depth [y-axis] and time [x-axis]). The depth and lateral resolution was approximately 16 μm and the time resolution was 1.25 ms.

Blood was again obtained using standard phlebology protocols and used without dilution (hct 44%). It was assumed that this blood was fully oxygenated. For some experiments, the blood was deoxygenated by the addition of sodium dithionite (Aldrich, St. Louis, MO, 2.5 mg/g blood). We did not monitor or stabilize the pH of the solution in experiments using sodium dithionite. A clear solution of hemoglobin (defined here as having no significant concentration of other erythrocyte components or blood plasma constituents) was obtained by dissolving 1.5 g bovine hemoglobin (Sigma, St. Louis, MO, H-2625) in 20 mL of isotonic saline to obtain a solution with the same hemoglobin concentration as blood at a hct of 25%. According to the manufacturer, the hemoglobin is primarily in the met-Hb form. This was also suggested by the visual observation that the solution was a dark red–chocolate brown, as opposed to the bright red of the oxy-Hb or the red-violet of deoxygenated blood (deoxy-Hb). Whole-blood or Hb solution was then loaded into a 200 μm thick cuvette and was irradiated at 10 ms pulse duration, 1.8 mm spot size and 8.8 J/cm^2 radiant exposure with the VersaPulse Cosmetic laser. The laser light was delivered via fiber and coupled into the OCT system using a cold mirror, so that the axes of both the OCT system and the laser were normal to the cuvette face. The setup was aligned so that the OCT system imaged blood at the center of the pump laser beam. *M*-scans consisting of 1200 *a*-scans (1.5 s in duration) were obtained. The signal from a photodiode viewing the blood sample was recorded with the OCT signal so that the time of laser onset in the *m*-scan could be determined.

Magnetic resonance imaging. Teflon tubes with an approximately 1 mm luminal diameter were filled with blood diluted with isotonic saline to 22% hct. Some tubes were irradiated with the 532 nm laser (10 ms pulse duration, 10 J/cm^2, 3 mm spot size) using sequential, slightly overlapping spots along the length of the tube. The tube ends were sealed, then the tubes were snap frozen in isopentane cooled with liquid nitrogen and stored on dry ice until the beginning of the MRI (approximately 2 h). Imaging was performed in a 9.4 T vertical bore MRI spectrometer (Bruker Instruments, Billerica, MA) in a 10 mm inner diameter radio frequency transmitter–receiver coil. Gradient-echo images were taken. Images showed cross sections of both native and irradiated blood-filled tubes. In sequential images, the echo time (TE) was increased from 8 to 30 ms. Images were obtained at constant relaxation time (TR) (1000 ms) and with varying TR (350–1000 ms).

Scanning electron microscope experiment. The structures of laser-generated coagula were investigated using a scanning electron microscope (SEM). Coagula were prepared by placing undiluted blood in a dish to a depth of about 4 mm and irradiating the exposed blood with 10 slightly overlapping shots from the 532 nm laser (10 ms pulse width, 10 J/cm^2, 3 mm spot size). Coagula were removed from the blood pool with forceps and placed in 10% formaldehyde solution overnight. The coagula were processed according to standard SEM procedures in successive grades of ethanol, critical point dried and sputter coated. Samples were then imaged with an SEM (JSM-820, Jeol, Peabody, MA).

RESULTS

Double-integrating sphere results

Figures 1–8 show data for the reflectance and total transmission of coagulating blood at probe wavelengths of 532, 594, 633, 675, 905 and 1064 nm. The data for 780, 820 and 980 nm are qualitatively very similar to the 905 and 1064 nm figures. Figures 2 and 3 are the undeflected transmission measurements of whole blood and an oxy-Hb solution at a probe wavelength of 594 nm. In this case the probe laser was too weak (~1 mW) to allow even direct-coupled integrating sphere measurements of the transmission and reflection to be made with the current experimental sensitivity. Figures 4 and 5 show data for whole blood and an oxy-Hb solution at a probe wavelength of 633 nm. The reflectance of the 532 nm pump laser is shown in each graph to show the extent of the pump laser pulse (10 ms) and to index the time base to the laser pulse and the onset of coagulation.

OCT results, *in vitro*

Figures 9–11 show OCT *m*-scans of irradiated met-Hb solution, oxy-Hb and deoxy-Hb, respectively. The horizontal axis is time, and the vertical axis is depth into the sample. The bright horizontal lines near the top and bottom of the images are the cuvette–blood

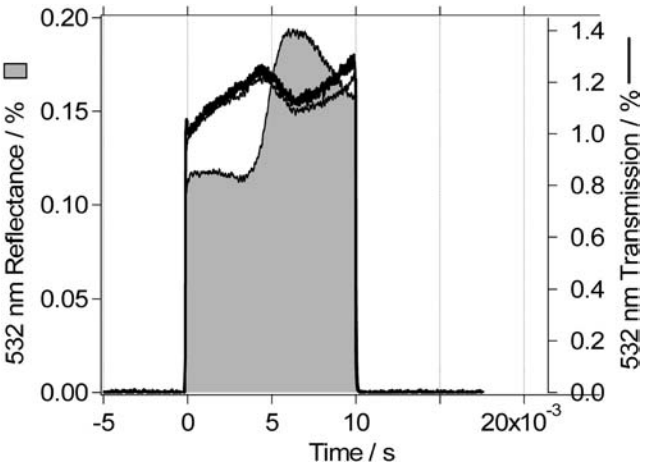

Figure 1. Diffuse reflectance (532 nm) (shaded line to zero), 532 nm total transmission (thick solid line) and deflected transmission (lower light solid line); 9 J/cm^2, whole-blood dilution and hct = 24.5%.

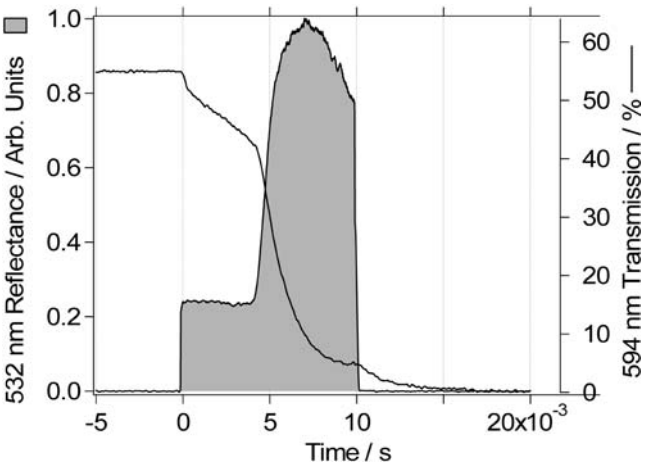

Figure 3. Diffuse reflectance (532 nm) (shaded line to zero) and 594 nm undeflected transmission (solid line); 14 J/cm^2, oxy-Hb solution and effective hct = 24.5%.

and blood–cuvette interfaces, respectively. Each figure is an average of 8 OCT *m*-scans from eight separate irradiations. Averaging allows features to be seen more clearly by mitigating noise and speckle effects.

MRI results

Figure 12 shows a sequence of images (a–d) of the cross section of two tubes, one filled with native (right) and one with laser-irradiated (left) blood. The TE was increased in successive images (left to right: 8, 12, 20 and 30 ms). The TR also increased in these images, from 350 to 1000 ms, although additional experiments showed that the variation in TR (at least in this range) had a negligible effect on the appearance of the images.

SEM results

Figures 13–15 show representative SEM images of the top (13) and bottom surface (14 and 15), respectively, of a laser-generated coagulum. Note the different magnifications in the images.

DISCUSSION

The discussion of the results will be done using the framework previously adopted (12), breaking down the coagulation into three distinct phases as shown schematically in Fig. 16.

Heating phase

The integrating sphere probe wavelengths in the experiment cover absorption features of oxy-, met- and deoxy-Hb. The data confirm our earlier conclusions that there are no chemical changes in the hemoglobin chromophore or structural changes in the components of the blood matrix to within the limits of our ability to detect them. There is no significant change in absorption for the wavelengths that are weakly absorbed by the target chromophore (oxy-Hb). There is no detectable evidence of photodissociation of oxy-Hb to deoxy-Hb during this phase, nor is there any evidence of photothermal deoxygenation. There is no detectable evidence of protein denaturation, defined as a significant increase in the scattering coefficient of the system probed both by the reflectance

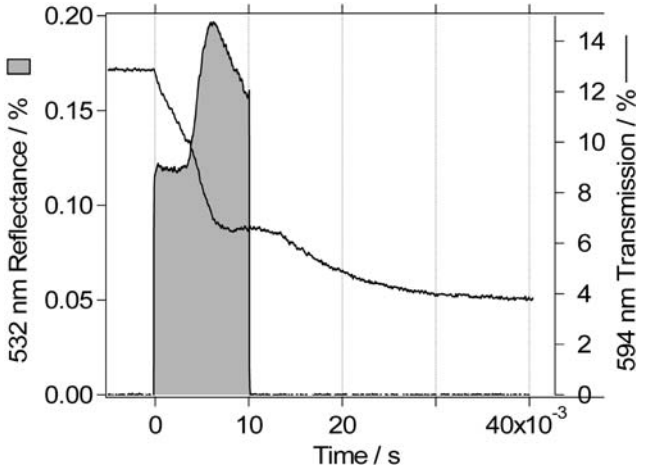

Figure 2. Diffuse reflectance (532 nm) (shaded line to zero) and 594 nm undeflected transmission (solid line); 9 J/cm^2, whole-blood dilution and hct = 24.5%.

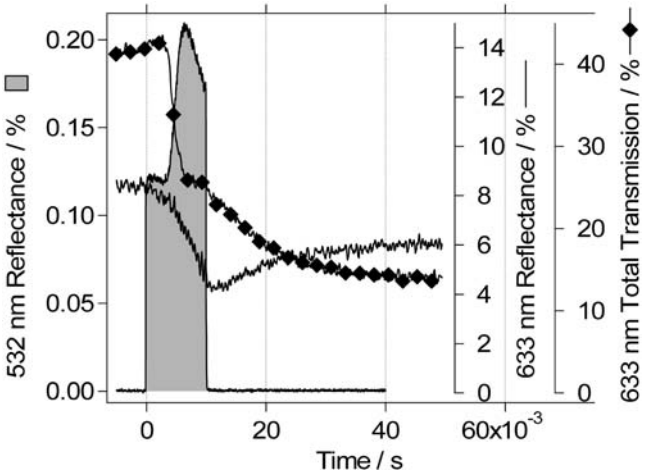

Figure 4. Diffuse reflectance (532 nm) (shaded line to zero), 633 nm total transmission (line with diamonds) and diffuse reflectance (solid line); 10 J/cm^2, whole-blood dilution and hct = 24.5%.

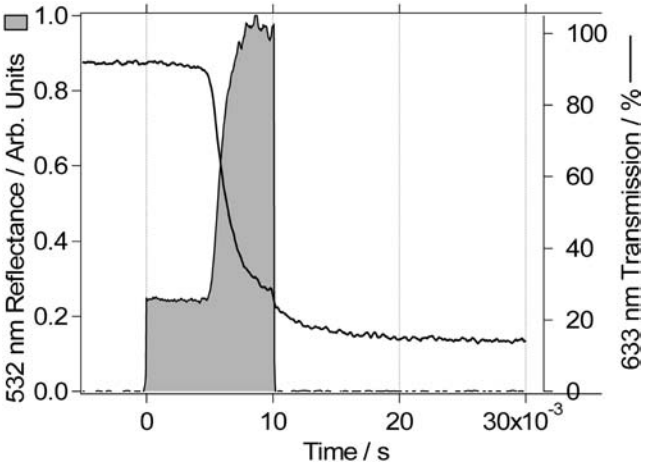

Figure 5. Diffuse reflectance (532 nm) (shaded line to zero) and 633 nm total transmission (solid line); 12 J/cm^2, oxy-Hb solution and effective hct ~24.5%.

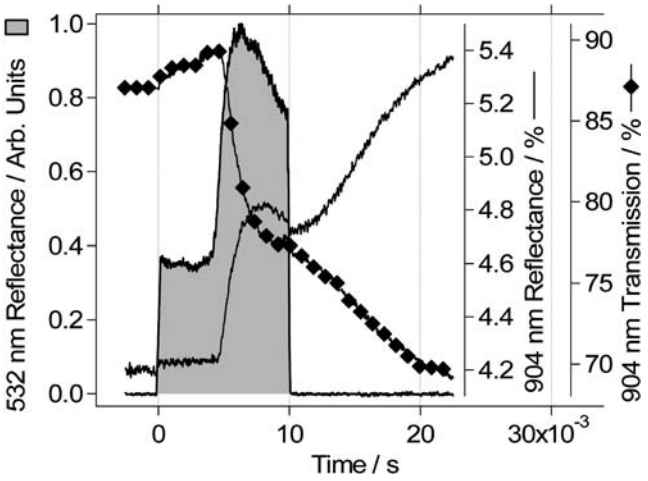

Figure 7. Diffuse reflectance (532 nm) (shaded line to zero), 904 nm total transmission (line with diamonds) and diffuse reflectance (solid line); 10 J/cm^2, whole-blood dilution and hct = 22%.

of the sample, and the time-domain OCT measurements. Our previous data (11), and that of Verkryusse *et al*. (22), indicated that the absorption coefficients of wavelengths on or close to resonance do change. Here, the transmission of 532 nm light increases as a function of the temperature of the sample (Fig. 1), and the transmission of 594 nm light decreases markedly (Figs. 2 and 3). Verkryusse *et al*. (22) showed that the transmission decreased at 585 nm. These observations reinforce our belief that during the heating phase a bathochromic (''red'') shift of the absorption features of the Hb chromophore dominates the optical properties of the sample. This bathochromic shift has been previously discussed (23–25), but because of the limitations of slow heating and denaturation, a maximum temperature of only 40°C was achieved. Our data indicate that absorption features of oxy-Hb continue to shift under rapid laser heating up to approximately 70°C (to the onset of primary coagulation) (12).

The physical origins of this bathochromic shift are described in detail in molecular spectroscopy texts (26). There are significant implications for the development of new therapeutic vascular lasers. To date it has been assumed that the penetration depths of light into the vessel could be predicted by *a priori* consideration of the room-temperature hemoglobin absorption spectrum. The argument is frequently made that 585, 595 and 600 nm lasers penetrate more deeply into the vessel than shorter wavelengths and, therefore, should be more effective at inducing photothermal sclerosis (3–8). This assumption is not correct, and furthermore the effect of the bathochromic shift is more pronounced on the steeper orange-red wing of the hemoglobin absorption spectrum. As the temperature rises, 532 nm light actually penetrates slightly more deeply into blood *in vitro*, whereas the penetration depths at the longer wavelengths *in vitro* decrease. This is exemplified in Figs. 2 and 3 where the 594 nm probe is extinguished. The effective absorption coefficient at this wavelength must increase by more than one order of magnitude during the heating and primary coagulation phases for this to happen.

Primary coagulation phase

After the heating phase the reflectance and transmission behaviors for all probe wavelengths change significantly at a time inversely proportional to the radiant exposure of 532 nm light and also

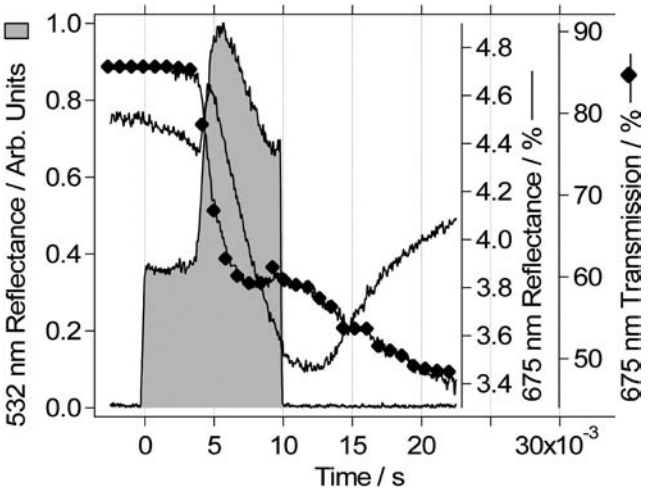

Figure 6. Diffuse reflectance (532 nm) (shaded line to zero), 675 nm total transmission (line with diamonds) and diffuse reflectivity (solid line); 10 J/cm^2, whole-blood dilution and hct = 22%.

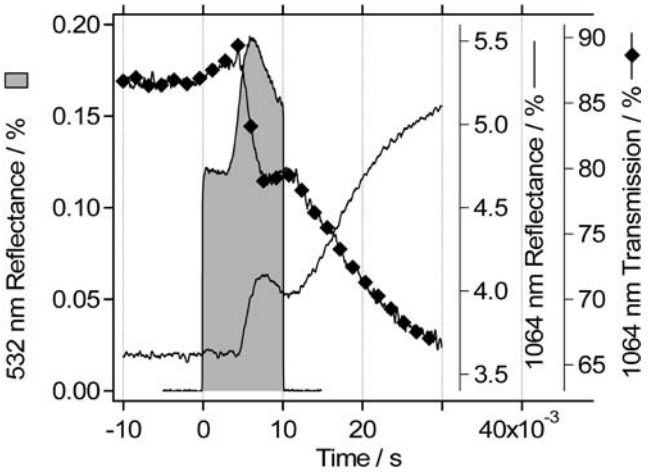

Figure 8. Calibrated 532 nm diffuse reflectance (shaded line to zero), calibrated 1064 nm total transmission (line with diamonds) and diffuse reflectivity (solid line); 10 J/cm^2, whole-blood dilution and hct = 24.5%.

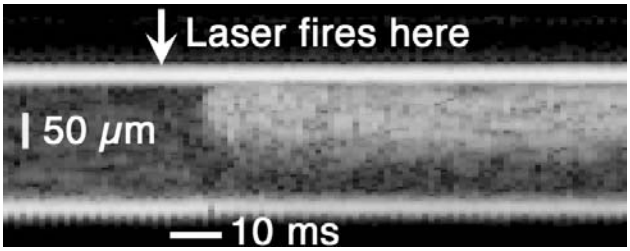

Figure 9. OCT *m*-scan of bovine met-Hb solution, 1.5 g/20 mL saline and irradiated with a 532 nm laser. Effective hct = 44%, 10 ms pulse duration, 1.8 mm spot size and 8.8 J/cm^2 radiant exposure.

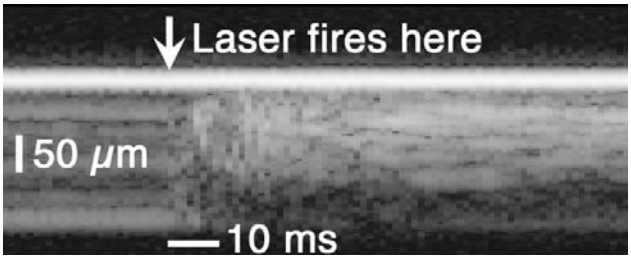

Figure 11. OCT *m*-scan of full-strength blood deoxygenated with sodium dithionite and irradiated with a 532 nm laser. Hct = 44%, 10 ms pulse duration, 1.8 mm spot size and 8.8 J/cm^2 radiant exposure.

dependent on the sample preparation. We call this the onset of the primary coagulation phase.

Primary coagulation phase sphere reflectivity data. At all probe wavelengths except 633 nm, and for all sample preparations, the reflectance increases at the onset of primary coagulation. At both 532 nm, and >780 nm a decrease in reflectance is seen approximately 7 ms after the beginning of the laser pulse. We have shown that one reaction pathway after laser activation is the chemical modification of oxy-Hb to met-Hb (11). The differences in reflectance for the different wavelengths can be partially explained by the difference in absorption of the two species, summarized in Table 1 (27–32).

At 532 nm the absorptivity of met-Hb is 60% of that of oxy-Hb. At 633 nm the absorptivity of met-Hb is approximately 27× greater than that of oxy-Hb. At longer probe wavelengths from 675 nm to 1064 nm, this ratio is smaller, ranging from 1.8 to 4.9 (27,28), and the absolute absorptivity of both chromophores is up to two orders of magnitude lower than at 532–633 nm. The 633 nm reflectance decreases significantly at coagulation, consistent with substantial conversion to met-Hb. At 675 nm and at longer wavelengths, the increased absorption from met-Hb and increased backscattering from the coagulum seem more closely balanced in their effects.

For 532 nm and >780 nm, a decrease in reflectance is observed toward the end of the heating laser pulse. During thermolysis of blood the erythrocytes transition from biconcave discs to spherocytes (33). Rupture of these swollen erythrocytes will yield a random ensemble of cell wall fragments without the coherent Mie scattering properties of a sample of similarly shaped objects. We believe that the most likely explanation for this decrease in reflectance is the bursting of the deformed RBCs (29,33,34).

Primary coagulation phase sphere transmission data. At all probe wavelengths the transmission decreases at the onset of primary coagulation. Development of a scattering coagulum affects the transmission of the various probe beams in two ways, both leading to an apparent decrease in transmission (34). First, the increase in backscattering decreases the likelihood that a photon can traverse the sample region and become a transmitted signal. Second, a scattering medium increases the effective pathlength in the sample because of the random-walk trajectory of the light, giving rise to increased absorption. Monte Carlo calculations show that the reduced scattering coefficient at 1064 nm would have to increase by approximately 15× to cause a comparable decrease in transmission (assuming constant absorption coefficient). The actual situation is more probably a combination of increased scattering and increased absorption from met-Hb generation.

The large decrease in transmission at 633 and 675 nm at the onset of coagulation can be attributed to met-Hb generation. It is also possible that the 675 nm result indicates a reaction channel, yielding deoxy-Hb. The increase in the absorption coefficient from 675 to 1064 nm resulting from oxy-Hb to met-Hb conversion ranges from 1.8 to 4.9×, and the 780–1064 nm results all look quite similar. However, the 675 nm results suggest a larger underlying increase in effective absorption coefficient. The absorption coefficient increase expected at 675 nm for oxy-Hb to deoxy-Hb is 6.3× (27), which might explain the observations. This highlights the advantages of using several different probe wavelengths with different sensitivity to the various molecular species.

The functional forms of the R–T data for 780, 820, 904, 980 and 1064 nm are practically mirror images of one another. At these weakly absorbed wavelengths the reflectances all increase at the onset of primary coagulation, and the transmissions all decrease. The temporal alignment of the major features of the R and T curves bolsters the idea that the molecular denaturation, RBC morphology changes and chemical changes occur almost simultaneously on this heating timescale. For whole blood at these dilutions and cuvette thicknesses, insufficient heating occurred at the deepest levels during the pump pulse to cause alteration through the whole sample (12). This is an important consideration when examining the integrating sphere data. The transmission data will include a contribution from native blood, but the reflectivity is a ''top-weighted'' probe of the sample sampling native blood to a lesser extent.

At the end of the primary coagulation phase the transmissions at 532 nm and from 675 to 1064 nm stop decreasing and then rise slightly in some cases. The rise at 532 nm is probably due to the underlying bathochromic shift in the absorption spectrum, which reduces the absorption coefficient at 532 nm. The slight rise in transmission at the longer near-infrared wavelengths is probably due to the rupture of the swollen spherocytes, which reduces the scattering losses.

Primary coagulation phase OCT data. The time-domain OCT measurements give a depth-resolved measure of reflectivity. The earliest increase in reflectivity occurs not at the cuvette–blood

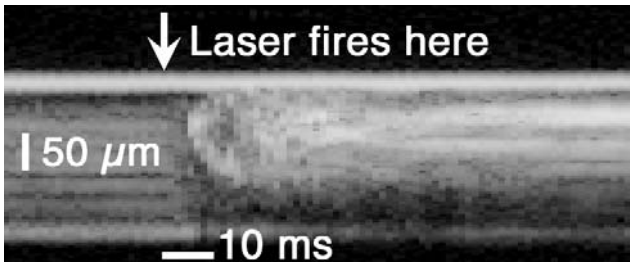

Figure 10. OCT *m*-scan of full-strength oxygenated blood irradiated with a 532 nm laser. Hct = 24.5%, 10 ms pulse duration, 1.8 mm spot size and 8.8 J/cm^2 radiant exposure. Note the bright ''C''-shaped region evolving around 50 μm into the cuvette at around 5 ms.

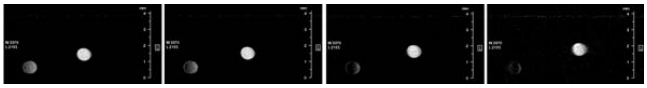

Figure 12. (a–d)MRI results (cross sections) for four different TE exposures of one native and one laser-irradiated blood-filled tube. The native blood tube is the right dot in each frame and the laser-irradiated tube is the lower left dot. From left to right, TE of (a) 8 ms, (b) 12 ms, (c) 20 ms and (d) 30 ms.

interface but approximately 50 μm deep into the sample. This is in good agreement with our thermal model (12) and is due to the fact that the cuvette wall initially acts as a heat sink. The hottest part of the sample in the model is 30–50 μm inside the wall. Features are seen in the oxy-Hb and deoxy-Hb data that are not seen in the hemoglobin solution. The Hb solution *m*-scan is consistent with a simple two-phase system, where the hemoglobin changes from a clear solution to a scattering or turbid solution on coagulation. The whole-blood samples are more complicated. Five to 7 ms after the onset of the laser pulse, a bright ''C''-shaped region is seen. This can be explained as a ''wave'' of denaturation, spreading both deeper and shallower from the initial temperature maximum at about 50 μm, causing shape changes in the erythrocytes (12,33). Intracellular denaturation of the Hb molecule is probably occurring during this period also, but the scattering coefficient change due to RBC shape alteration appears to dominate the OCT data.

We have eliminated several other possible explanations. For example we have seen bubbles in the sample due to vaporization (steam formation) at excessive fluences. A suggestion that the C-shaped region was caused by oxygen microbubbles released by the erythrocytes is undermined by the deoxy-Hb data, which still shows the feature. It is also contraindicated by the time-domain thermal measurement technique, which is extremely sensitive to the presence of bubbles (12). Throughout this study we have seen no evidence for oxygen bubbles. This is surprising because an erythrocyte can complex a volume of oxygen 20× its own volume, and one might expect this to be liberated under these shock heating conditions. The liquid phase is also getting very hot during photocoagulation, and Henry's law dictates that the solubility of gases in water decreases with elevated temperature. We do not currently understand the final destination of the complexed oxygen. Liberation of solvated superoxide ions could be one possibility (35). In this respect our results differ from those of Halldorsson, who observed bubbles when heating blood in a slow thermal bath experiment (31).

A second possible explanation is that the OCT experiments are seeing regions with substantial refractive index gradients resulting from differential heating of the sample. We have shown as a by-product of our study of the thermal properties of the sample that the heating gradients generated are insufficient and of the wrong shape to account for the C-shaped region (12).

MRI data. Met-Hb generation has been identified as a reaction product of thermally denatured blood by a number of groups (15–17,36,37) and as a by-product of blue and ultraviolet light irradiation by Demma and Salhany (35) and Kollias *et al.* (38). This is the first time visible laser irradiation has been shown to generate the species in detectable concentration. Farahani *et al.* measured the temperature correlation between the decrease of the longitudinal spin relaxation time T_1 and the increase in absorption of blood samples at 630 nm, both indicative of met-Hb generation (17). They found that a critical temperature of 60°C was required to produce these signatures. A similar result has recently been found by Graham *et al.* (36) using MR and Alves and Wajnberg using electron paramagnetic resonance (14). Met-Hb has been suggested for use as an MRI contrast-enhancing agent by Duewell *et al.* (39). The authors of the study calculated the steady-state concentration (25%) at which met-Hb would become useful as a contrast agent. Assuming that our hypothesis of met-Hb formation is correct, we may calculate the volume fraction of met-Hb produced photothermally. The drop in transmission at 1064 nm in the primary coagulation phase (Fig. 8) indicates that 70–80% of the oxy-Hb in the irradiated volume of blood is converted to met-Hb using millisecond 532-nm irradiation. This percentage conversion satisfies the Duewell criterion for visible contrast.

Hospital-acquired acute renal failure is an increasingly common problem in contemporary healthcare and is associated with a high mortality rate. Radiocontrast-induced nephropathy (RCIN), including iodine-based solutions given during X-ray fluoroscopy, and Gd-based agents in MRI is the third most common underlying cause of this complication and is on the rise because of the

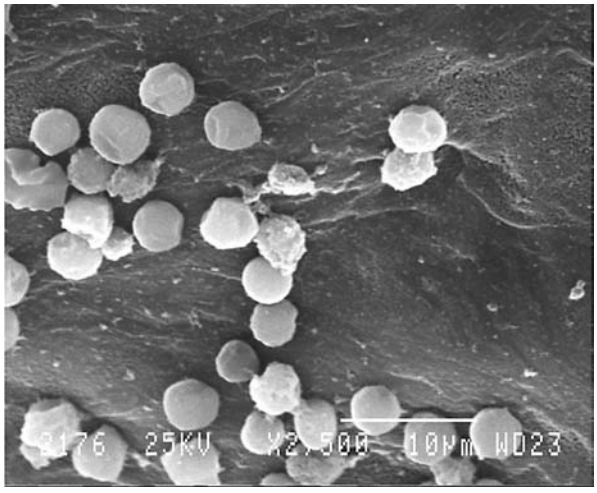

Figure 13. SEM image of the top (laser-irradiation side) surface of a laser-generated coagulum. Scattered erythrocytes on the surface are believed to be cells that were not washed off during the preparation process.

Figure 14. SEM image of the surface of a laser-generated coagulum opposite to the laser irradiation side showing aggregation of spherocytes.

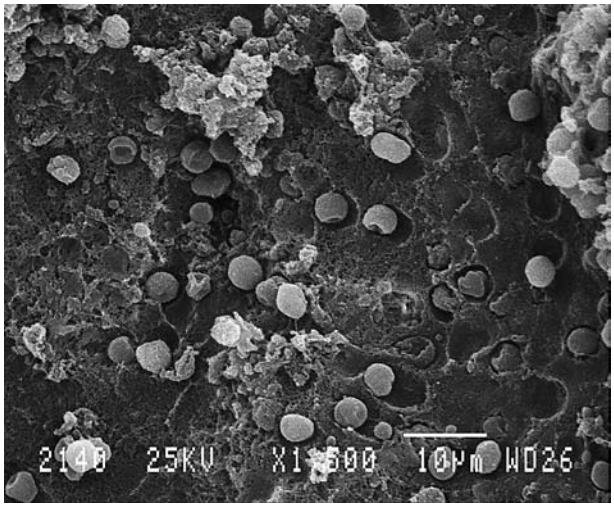

Figure 15. SEM image of the bottom surface of a laser-generated coagulum showing pockets developing around spherocytes.

increasing incidence of heart-related illnesses in the Western world (40). Major risk factors for RCIN include chronic renal insufficiency, diabetes mellitus, any condition associated with decreased effective circulating volume, and use of large doses of contrast media. Chelated Gd-based MRI agents are also known to cause interference with standard serum assays of important cations such as Ca, Fe, Mg and Zn (41).

Met-Hb offers several intriguing advantages for the generation of *in vivo* MRI contrast. It is formed from a naturally occurring body chemical, is well tolerated in the vascular system (39), and is naturally removed by enzymes in the body. We may generate the contrast bolus locally using a catheter rather than systemically, and in a time-domain manner inside the magnet because the laser is delivered to the patient by nonmagnetic fiberoptic means. Laser-generated contrast may also ameliorate the need for extended drug-path clinical trials because the implementation is a device rather than exogenous chemical injection, and conceivably we may couple the diagnostic and therapeutic potential of lasers to the treatment site in the same fiber, minimizing the number of interventions needed and trauma to the patient.

Our initial data using laser-induced met-Hb production for MRI contrast are encouraging. Figures 12a–d show that the native blood

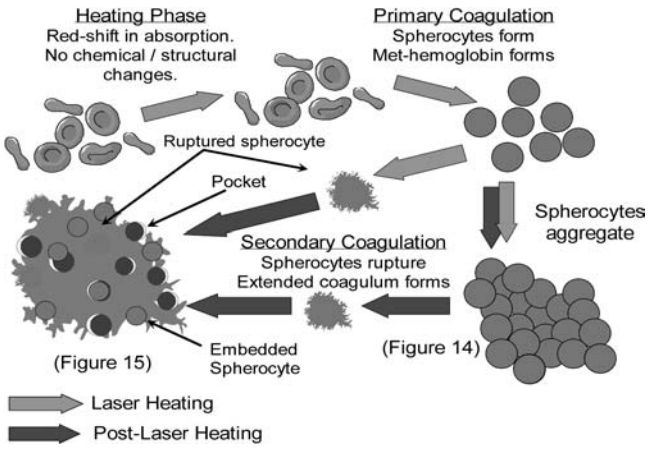

Figure 16. Schematic illustration of the processes involved in *in vitro* laser photocoagulation of blood.

Table 1. Absorption coefficients (cm^{-1}) of oxy-Hb, deoxy-Hb and methemoglobin compiled from various sources (23–25,27–32). All values have been scaled to hct = 24.5%

Absorption coefficient (cm^{-1})	532 nm	594 nm	632 nm	675 nm	904 nm	1064 nm
Oxy-Hb	117	22	1.5	1.1	3.1	1.4
Deoxy-Hb	86	60	13	6.9	2.2	0.35
Met-Hb	70	35	41	3.7	6.7	6.8

remains at near-constant intensity as the TE interval is increased, whereas the laser-irradiated blood becomes progressively hypointense. The images confirm that laser-irradiated blood has a higher susceptibility than native blood. Using T_1-weighted images we may generate hyperintense images, which are of more practical value in a clinical setting. These images also have the advantage of being faster to collect, making this technique more useful for time-domain investigations such as measurements of cardiac performance, perfusion of tumors or skin grafts and the evaluation of neural ischemia (stroke) and myocardial infarction (heart attacks).

The results given here are from tubes of blood irradiated multiple times. Unfortunately, we were unable to image a localized, single laser–induced coagulum for comparison with the integrating sphere data. Although the samples were frozen during transport between laser irradiation and the MRI spectrometer, the setup time was sufficiently long that the samples thawed, the coagulum disintegrated and mixed with the native blood. The met-Hb formed from a single coagulum, distributed throughout the large tube volume, did not cause a recognizable signal change. Future studies will involve fiber transmission of the laser light into the MR instrument and rapid imaging of a single cross section through the irradiated blood. Other MR pulse sequences will also be tested. Another area of inquiry is to determine the signal level in a lower field strength instrument (clinical MRI instruments are typically 1 T).

Secondary coagulation phase

The optical properties of irradiated whole blood continue to evolve even after the pump laser pulse is removed. We term this the secondary coagulation phase. Examination of the time-domain thermal properties of the system show that the ''disc'' of heated blood remains hot long after the laser pulse terminates (12), so temperature-mediated reactions can still take place.

The features of the secondary coagulation phase are similar for all probe wavelengths in the sphere experiments. The transmissions drop, while the reflectances increase. As with the primary phase data, the 780–1064 nm R–T data are almost mirror images. The optical properties in the secondary coagulation phase seem to stabilize approximately 50 ms after the end of the pump pulse. We have followed the signals out to approximately 100 ms, after which convection in the sample starts to perturb the measurements. These secondary coagulation features are not present when the target is a solution of oxy-Hb (Figs. 3 and 5). They are present but quite diminished if the target is a suspension of erythrocytes that have been repeatedly washed in isotonic saline and then centrifuged to remove the components of the blood plasma. The time-domain OCT measurements show the formation of a secondary coagulum as a second region of relatively high backscattering forming shortly after the end of the laser pulse. This second region appears to

stabilize approximately 40–50 ms after the end of the laser pulse, in agreement with integrating sphere reflectance data.

We infer from the above that the secondary phase of coagulation in whole blood *in vitro* is dominated by the aggregation of a macroscopic coagulum composed of denatured hemoglobin and other plasma proteins (fibrin etc.) and the cell membranes of ruptured erythrocytes. We believe that the dominant influence on the optical properties comes from the change in the scattering coefficient of the system resulting from the emergence of this macroscopic coagulum.

Scanning electron microscopy data

The SEM pictures (Figs. 13–15) of a laser-generated macroscopic coagulum are interesting with respect to the discussion of the secondary phase. The top (laser illumination) surface of the coagulum (Fig. 13) appears smooth, consistent with protein ''melting'' at the high temperatures anticipated at this level. We have previously calculated a peak temperature of 92°C at the top surface of a coagulum formed in a glass cuvette (12). Although the thermal boundary condition in this case (air) is different, temperatures at least as high would be expected (42). Several RBCs are seen on the top surface of the coagulum. Because they appear to be resting on top of the coagulum, we believe that this is contamination that occurred during the process of lifting the coagulum from the dish and transferring it to the fixative solution.

The bottom surface of the coagulum (Figs. 14 and 15) has a different appearance, with ''intact'' RBCs and spherocytes fused together or entrained in a denatured protein meshwork. The peak temperature at the bottom of the coagulum is lower than at the top, so this view shows many of the intermediate steps in coagulum formation. The cells range in shape from distorted biconcave discs to spheroids to wrinkled fragments. This is in line with previous observations that heated RBCs change form from biconcave to spheroid, causing an increase in backscatter, then rupture causing a decrease in scattering (33). Figure 14 may also show another mechanism for the scattering decrease. RBCs fusing into tight clusters as seen in this image will cause displacement of blood plasma and subsequent index matching that will decrease scattering. It would still be expected that at higher temperatures or longer heating times (or both) the RBC membranes in these clusters would burst.

Overall picture

The interaction of a laser with blood in vascularized tissue to cause photothermal sclerosis is a complicated process involving hemodynamics, structural elements of the blood vessels themselves, oxygenation ratios in the blood, multidimensional heat transfer processes and thermally induced biochemical processes in the endothelial cells of the blood vessel (1–9,18,19,43). Two simplifying conjectures applied to the design of dermatologic vascular lasers are (a) to assume penetration depths calculated using the optical properties and spectroscopy of room-temperature blood *in vitro*, and from there calculate optimum laser wavelengths and (b) to assume two-dimensional (planar) heat diffusion away from a cylindrical vessel embedded in a homogenous conductive medium and from that extract the optimum pulse duration (43).

The bathochromic shift, conversion to met-Hb, RBC shape changes and protein denaturation we have described all appear to be thermally induced, and so will probably occur for all laser parameters producing a photothermal effect. Preliminary integrating sphere data obtained at 2 and 50 ms pulse durations appear to show the same features as seen at 10 ms, indicating that these phenomena hold over at least an order of magnitude in pulse duration and so potentially cannot be ignored for treatment of either small or large vessels (22,43). From our experiments, it is clear that arguments based on the optical properties of ''cold'' blood *in vitro* will fail. At 532 nm, both the bathochromic shift and the conversion to met-Hb will increase laser light penetration depth in blood as a function of temperature. This may be offset by the increase in scattering due to Hb coagulation and RBC shape changes. The situation is much worse for orange-red wavelengths. Here, the bathochromic shift, met-Hb production and scattering increases may all combine to severely attenuate penetration of light into the blood vessel.

Another consideration linked to an abrupt change in optical properties for a given wavelength is that of dosimetry. Recent results treating PWS with highly penetrating 1064 nm laser light have indicated that full-thickness burns can occur even with careful selection of laser parameters (9). We believe that one possible explanation for this is the abrupt increase in absorption at 1064 nm resulting from the met-Hb conversion. Beyond this point the radiant exposure is too high to allow the heat generated to dissipate into the bulk on a compatible timescale (43), and the result is collateral perivascular damage. Probe lasers (630–635 nm) incorporated into the therapeutic laser as interlocked safety devices could serve as diagnostics of the onset of met-Hb generation to ameliorate the chances of such complications.

CONCLUSIONS

We have performed optical, OCT and MRI experiments to study the processes occurring as blood is photothermally denatured. These results substantiate our earlier hypotheses about the mechanisms of coagulation during 10 ms 532 nm laser irradiation. We have provided evidence of Hb absorption spectrum shifts, RBC shape changes and coagulation on both molecular and macroscopic scales. The depth- and time-resolved capability of OCT is crucial to observe the propagation of coagulation ''waves'' through the sample. Finally, the MR images provide further evidence of the presence of met-Hb in coagulated blood and suggest the potential for laser-induced met-Hb as an MRI contrast agent.

Acknowledgement—We thank Dr. Rox Anderson and Prof. A. J. Welch for helpful discussions, Dr. Ted Trouard for his assistance with the MRI experiments and Stuart Loui for his assistance in obtaining the SEM samples and images. This work was partially supported by a grant from the National Institutes of Health (CA83148).

REFERENCES

1. Anderson, R. R. and J. A. Parrish (1981) Microvasculature can be selectively damaged using dye lasers: a basic theory and experimental evidence in human skin. *Lasers Surg. Med.* **1**, 263–276.
2. Anderson, R. R. and J. A. Parrish (1983) Selective photothermolysis: precise microsurgery by selective absorption of pulsed radiation. *Science* **220**, 524–527.
3. Hsia, J., J. A. Lowery and B. Zelickson (1997) Treatment of leg telangiectasia using a long-pulse dye laser at 595 nm. *Lasers Surg. Med.* **20**, 1–5.
4. Bernstein, E. F., S. Kornbluth, D. B. Brown and J. Black (1999) Treatment of spider veins using a 10 millisecond pulse-duration frequency-doubled neodymium YAG laser. *Dermatol. Surg.* **25**, 316–320.
5. Kienle, A. and R. Hibst (1995) A new optimal wavelength for treatment of port wine stains? *Phys. Med. Biol.* **40**, 1559–1576.

6. van Gemert, M. J. C., A. J. Welch, J. W. Pickering, O. T. Tan and G. H. M. Gijsbers (1995) Wavelengths for laser treatment of port wine stains and telangiectasia. *Lasers Surg. Med.* **16**, 147–155.
7. Tan, O. T., S. Murray and A. K. Kurban (1989) Action spectrum of vascular specific injury using pulsed irradiation. *J. Invest. Dermatol.* **92**, 868–871.
8. Hohenleutner, U., T. Walther, M. Wenig, M. Baumler and M. Landthaler (1998) Leg telangiectasia treatment with a 1.5 ms pulse due laser, ice cube cooling of the skin and 595 vs. 600 nm: preliminary results. *Lasers Surg. Med.* **23**, 72–78.
9. Yang, M. U., A. N. Yaroslavsky, W. A. Farinelli, S. S. Tsao and R. R. Anderson (2003) Long-pulsed Nd:YAG laser treatment for port wine stains. *Lasers Surg. Med.* **32 S15**, 28.(Abstract 90)
10. Cain, C. P., G. D. Noojin and L. Manning (1986) A comparison of various probit methods for analyzing yes/no data on a log scale. U.S.A.F. Rep. AL/OE-TR-1996-0102.
11. Barton, J. K., G. Frangineas, H. Pummer and J. F. Black (2001) Cooperative phenomena in two-pulse, two-color laser photocoagulation of cutaneous blood vessels. *Photochem. Photobiol.* **73**, 642–650.
12. Barton, J. K., D. Popok and J. F. Black (2001) Thermal analysis of blood undergoing laser photocoagulation. *IEEE J. Sel. Topics Quant. Electron.* **7**, 936–943.
13. Barton, J. K., A. Rollins, S. Yazdanfar, T. J. Pfefer, V. Westphal and J. A. Izatt (2001) Photothermal coagulation of blood vessels: a comparison of high-speed optical coherence tomography and numerical modeling. *Phys. Med. Biol.* **46**, 1665–1678.
14. Alves, O. C. and E. Wajnberg (1993) Heat denaturation of met-Hb and HbNO: e. p.r evidence for the existence of a new hemichrome. *Int. J. Biol. Macromol.* **15**(5), 273–279.
15. Seto, Y., M. Kataoka and K. Tsuge (2001) Stability of blood carbon monoxide and hemoglobins during heating. *Forensic Sci. Int.* **121**(1–2), 144–150.
16. Randeberg, L., A. Daae Hagen and L. Svaasand (2002) Optical properties of human blood as a function of temperature. *Proc. SPIE* **4609**, 20–28.
17. Farahani, K., R. E. Saxton, H-C. Yoon, A. A. F. De Salles, K. L. Black and R. B. Lufkin (1999) MRI of thermally denatured blood: methemoglobin formation and relaxation effects. *Magn. Reson. Imaging* **17**, 1489–1494.
18. Ahan, U., P. Zorman, D. Recek, S. Ralca and B. Majaron (2004) Port wine stain treatment with a dual-wavelength Nd:YAG laser and cryogen spray cooling: a pilot study. *Lasers Surg. Med.* **34**(2), 164–167.
19. Mordon, S., D. Brisot and N. Fournier (2003) Using a ''non-uniform pulse sequence'' can improve selective coagulation with an Nd:YAG laser (1. 06 μm) thanks to met-hemoglobin absorption: a clinical study on blue leg veins. *Lasers Surg. Med.* **32**, 160–170.
20. Pickering, J. W., S. A. Prahl, N. van Wieringen, J. F. Beek, H. J. C. M. Sterenborg and M. J. C. van Gemert (1993) Double-integrating-sphere system for measuring the optical properties of tissue. *Appl. Opt.* **32**, 399–410.
21. Rollins, A. M., M. D. Kulkarni, S. Yazdanfar, R. Ung-arunyawee and J. A. Izatt (1998) *In vivo* video rate optical coherence tomography. *Opt. Express* **3**, 219–229.
22. Verkryusse, W., A. M. K. Nilsson, T. E. Milner, J. F. Beek, G. W. Lucassen and M. J. C. van Gemert (1998) Optical absorption of blood depends on temperature during a 0.5 ms laser pulse at 586 nm. *Photochem. Photobiol.* **67**, 276–281.
23. Cordone, L., A. Cupane, M. Leone and E. Vitrano (1986) Optical absorption spectra of deoxy- and oxyhemoglobin in the temperature range 300–320 K. *Biophys. Chem.* **24**, 259–275.
24. San Biagio, P. L., E. Vitrano, A. Cupane, F. Madonia and M. U. Palma (1977) Temperature induced difference spectra of oxy and deoxy hemoglobin in the near-IR, visible and Soret regions. *Biochem. Biophys. Res. Comm.* **77**, 1158–1165.
25. Steinke, J. M. and A. P. Shepherd (1992) Effects of temperature on optical absorbance spectra of oxy-, carboxy- and deoxy-hemoglobin. *Clin. Chem.* **38**, 1360–1364.
26. Atkins, P. W. (1983) Molecular Quantum Mechanics, second edition, Oxford University Press, Oxford, UK.
27. Zijlstra, W. G., A. Buursma and O. W. van Assendelft (2000) *Visible and Near Infrared Absorption Spectra of Human and Animal Haemoglobin.* VSP Publishing, Utrecht, The Netherlands.
28. Kuenster, J. T. and K. H. Norris (1994) Spectrophotometry of human hemoglobin in the near-infrared region from 1000 to 2500 nm. *J. Near Infrared Spectrosc.* **2**, 59–65.
29. Roggan, A., M. Friebel, K. Dorschel, A. Hahn and G. Muller (1999) Optical properties of circulating human blood in the wavelength range 400–2500 nm. *J. Biomed. Opt.* **4**, 36–46.
30. van Gemert, M. J. C., A. J. Welch and A. P. Amin (1986) Is there an optimal treatment for port wine stains. *Lasers Surg. Med.* **6**, 76–83.
31. Halldorsson, T. (1981) Alteration of optical and thermal properties of blood by Nd:YAG laser irradiation. In *Proceedings of the 4th Congress of the International Society for Laser Surgery*; Tokyo, Japan; 23–27 November (Edited by K. Atumi and N. Ninsakul).
32. Prahl, S. Optical absorption spectra of hemoglobin. Available at: http://omlc.ogi.edu/spectra/hemoglobin/index.html, accessed 18 June 2004.
33. Nilsson, A. M. K., G. W. Lucassen, W. Verkryusse, S. Andersson-Engels and M. J. C. van Gemert (1997) Changes in optical properties of human whole blood *in vitro* due to slow heating. *Photochem. Photobiol.* **65**, 366–373.
34. Prahl, S. A., M. J. C. van Gemert and A. J. Welch (1993) Determining the optical properties of turbid media by using the adding-doubling method. *Appl. Opt.* **32**, 559–568.
35. Demma, L. S. and J. M. Salhany (1977) Direct generation of superoxide anions by flash photolysis of human oxyhemoglobin. *J. Biol. Chem.* **252**, 1226–1230.
36. Graham, S. J., G. J. Stanisz, A. Kecojevic, M. J. Bronskill and R. M. Henkelman (1999) Analysis of changes in MR properties of tissues after heat treatment. *Magn. Reson. Med.* **42**, 1061–1071.
37. Fechner, G. G. P. and D. J. Gee (1998) Study on the effects of heat on blood and on the post-mortem estimation of carboxyhaemoglobin and methaemoglobin. *Forensic Sci. Int.* **40**, 63–67.
38. Kollias, N., A. Baqer, I. Sadiq and R. M. Sayre (1992) *In vitro* and *in vivo* ultraviolet-induced alterations of oxy- and deoxyhemoglobin. *Photochem. Photobiol.* **56**, 223–227.
39. Duewell, S., C. E. Kasserra, P. Jezzard and R. S. Balaban (1996) Evaluation of methemoglobin as an autologous intravascular MRI contrast agent. *Magn. Reson. Med.* **35**, 787–789.
40. Krämer, B. K., M. Kammerl, F. Schweda and M. Schreiber (1999) A primer in radiocontrast-induced nephropathy. *Nephrol. Dial. Transplant.* **14**, 2830–2834.
41. Proctor, K. A. S., L. V. Rao and W. L. Roberts (2004) Gadolinium magnetic resonance contrast agents produce analytic interference in multiple serum assays. *Am. J. Clin. Pathol.* **121**(2), 282–292.
42. Pfefer, T. J., B. Choi, G. Vargas, K. M. McNally and A. J. Welch (2000) Pulsed laser-induced thermal damage in whole blood. *J. Biomech. Eng.* **122**, 196–202.
43. Dierickx, C. C., J. M. Casparian, V. Venugopalan, W. A. Farinelli and R. R. Anderson (1995) Thermal relaxation of port-wine stain vessels probed *in-vivo*: the need for 1–10 millisecond laser pulse treatment. *J. Invest. Dermatol.* **105**, 709–714.